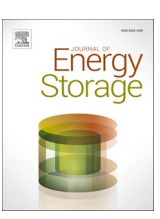
ELSEVIER

Contents lists available at ScienceDirect

Journal of Energy Storage

journal homepage: www.elsevier.com/locate/est



Research Papers



A scaling rule for power output of salt hydrate tablets for thermochemical energy storage

Martina Cotti a,b, Hartmut Fischer c, Olaf Adan b,c, Henk Huinink a,b,*

- a Eindhoven Institute of Renewable Energy Systems, Eindhoven University of Technology, PO Box 513, Eindhoven 5600 MB, the Netherlands
- b Transport in Permeable Media Group, Department of Applied Physics, Eindhoven University of Technology, PO Box 513, Eindhoven 5600 MB, the Netherlands
- ^c TNO Materials Solutions, High Tech Campus 25, 5656 AE Eindhoven, the Netherlands

ARTICLE INFO

Keywords: Salt hydrates Heat storage Tablets Power output Hydration kinetics Water vapor diffusion

ABSTRACT

Salt hydrates are thermochemical materials capable of storing and releasing heat through reversible reaction with water vapor. In a heat battery, salt hydrate tablets of millimeter size are necessary to ensure a sufficient permeability of the packed bed. A profound understanding of the hydration process of these tablets is required to improve their kinetic performance. In this study we show that the hydration timescale of salt tablets is transport limited and that it depends primarily on the porosity and on the driving force (Δp) . From gravimetric measurements done on SrBr₂·6H₂O and CaC₂O₄ we derived the intrinsic reaction and effective diffusion coefficients $(k \text{ and } D_{eff})$ and found that they validate a front-diffusion limited hydration hypothesis. In particular, the obtained D_{eff} values (0.8-4.5 mm² s⁻¹) only depend on the tablets' porosities. Based on these parameters, we calculated the second Damköhler number (Da_{II}) and proved that many other hydration reactions are diffusion limited. In the case of identical structures, the power output is therefore controlled only by the driving force. Its variation could be predicted by calculation of a so-called power scaling factor (Λ) for a selection of salts. This power scaling factor depends on the enthalpy (ΔH) and entropy (ΔS) of the reaction. For a temperature output of 40 °C and at 12 mbar most hydration reactions fall in the interval $0 < \Lambda < 30$ and Λ exceeds 30 only in very few cases. This parameter establishes therefore another important constraint to the selection of the most ideal salt. Suitable strategies to circumvent the diffusion limitation will lead to the development of next generation salt hydrate tablets for thermochemical energy storage.

1. Introduction

The development of groundbreaking, flexible and cheap energy storage systems is pivotal to the widespread use of renewable energy and to the achievement of effective energy management. Despite the most well-known energy storage system is the electric battery, heat is actually the most used form of energy, as it results from the analysis of the energy consumption of the three main economic sectors (industry, transportation and housing) [1]. Indeed, heat can be stored as sensible, latent heat or as chemical energy [2]. Within the latter category, thermochemical energy storage (TCES) indicates chemical reactions that allow to store and regenerate heat. For example, during the reaction of salt with water vapor, heat is released (hydration). When heat is supplied to separate salt from water (dehydration), energy can be stored indefinitely.

The selection process of the appropriate hydration reaction is determined mostly by the application conditions – discharging and charging temperatures that can be achieved in a determined setting. For [3,4], SrBr $_2$ and CaC $_2$ O $_4$ are the most promising salts for medium temperature applications (100-200 °C) because they show a small reaction hysteresis and a high cycling stability. SrBr $_2$ H $_2$ O hydration to hexahydrate is also identified as a good candidate for applications in the low temperature – or domestic – range (50-100 °C) for the same reasons by [5]. In the same temperature window we also find K $_2$ CO $_3$ and Na $_2$ S which have made it to the best 25 candidates of Donkers et al. [6] because of their high energy density. Some salts may not make it to the final selection due to concerns about their chemical stability (halide salts usually, [7]), but this may change if their chemical decomposition can be hampered [8]. In fact, several of these salts made it already to the salt battery level, as for example MgCl $_2$ [9] and SrCl $_2$ [10].

E-mail address: h.p.huinink@tue.nl (H. Huinink).

^{*} Corresponding author at: Eindhoven Institute of Renewable Energy Systems, Eindhoven University of Technology, PO Box 513, Eindhoven 5600 MB, the Netherlands.

In the earliest laboratory tests, salt batteries were usually filled with salt powders [11,12], which have a poor permeability for gases. This has triggered the development of millimeter size porous salt particles [10,13], which leads to particle beds with a much higher permeability. These mm-size particles can be irregular or geometrical in shape, and in order to avoid confusion, the latter will be called tablets from now on. Mm-size particles are typically obtained by various methods from µmsize powders [10,13–17]. There have been multiple attempts to make mm-size composite particles, with the aim to conjugate a newly achieved mechanical stability with additional functionalities in support of mass and heat transfer. For example, the concentration of expanded graphite (EG) was tested in several instances to increase the mechanical stability of salts' tablets during cycling, while encouraging mass transfer and increasing heat transfer across the tablet [14-16,18,19]. On top of that, certain hydrophilic agents have been researched to improve sorption properties, such as polyelectrolytes (PDAC) [14] or octylphenol polyoxyethylene(10) [15]. Salts and functional additives could be mixed together also by impregnation [20-24]. In these mm-size particles, salts are confined in a porous matrix and potentially both the enthalpy of hydration and of solution could be stored. So far promising candidates for use as porous matrixes are vermiculite [20,22] and certain polymeric matrixes [21,25].

The hydration kinetics of salt powders have been the subject of several studies, from fundamental to modelling [26–32]. It is known that hydration kinetics are controlled by either nucleation of the product phase or growth. Further, increasing experimental evidence supports that hydration is a liquid mediated process [26,27] and that kinetics are linked to the increasing porosity [29] and to cycling [33]. These achievements have led to several attempts to increase the hydration kinetics [34,35]. Modelling of these processes starts from a long history of solid-gas reaction modelling [36,37]. Far from equilibrium, good agreements in between experiments and models are in fact obtained by parametrizing the hydration rate according to a general 'Arrehenius-f (α)' model [22,28,31,38]. Close to equilibrium, other methods need to be used [39].

On the contrary, the kinetics of water absorption in a mm-size porous salt particle are less understood. Recently, Aarts et al. [40], have presented an in depth study on tablets of K₂CO₃·1.5H₂O. It was found that hydration of pure K₂CO₃ tablets is limited by water vapor diffusion through the pore system and that the structural properties of the particles (size and shape, porosity, tortuosity) were the most relevant parameters. Since the focus of the work of Aarts et al. is one very specific system, the applicability of these findings to other porous salt particles is unclear. This is why in this paper we would like to assess the generality of the model proposed by Aarts et al. by identifying reaction or diffusion limited hydrations among tablets made of other salts. The presented study focuses on the first (de)hydration cycle of pure salt tablets, and detailed particle compositions and stability are beyond its scope. Ultimately, we wish to establish if in general all pure salt tablets are diffusion limited and consequently highlight which salt hydrates make the highest power output tablet.

We start by examining the hydration kinetics of tablets made of $SrBr_2 \cdot 6H_2O$ and CaC_2O_4 with focus on two single transition reactions:

$$SrBr_2{\cdot}H_2O_{(s)} + 5{\cdot}H_2O_{(g)}{\rightleftarrows}SrBr_2{\cdot}6H_2O_{(s)}$$

$$CaC_2O_{4(s)} + H_2O_{(g)} \rightleftarrows CaC_2O_4 \cdot H_2O_{(s)}$$

Firstly, the hydration kinetics of the two reactions are evaluated at the powder level to extract an intrinsic reaction constant. This is used to estimate the second Damköhler number and to distinguish reaction limited from diffusion limited kinetics. Secondly, the hydration kinetics of cylindrical $\rm SrBr_2$ and $\rm CaC_2O_4$ tablets are evaluated with respect to the porosity of the tablets and the thermodynamic driving force. Because of the chosen experimental settings, we make use of the 1D diffusion model previously used by [40], calculate the diffusion coefficient and verify the existence of diffusion limitations. At last, from our experimental input

and the model, we find that other hydration reactions at the tablet level are diffusion limited. For these reactions, the diffusion limitation sets a barrier to the variation of power output. However, the power output may still change from salt to salt. This aspect is investigated starting from the diffusion model itself. Because it excludes any influence due to the structure, the outcome of the calculation is a scaling factor, Λ . The scaling factor was evaluated at one temperature and water vapor pressure and gave insight over the role of thermodynamic quantities (ΔH and ΔS) in determining the spread in power output. The scaling factor therefore represents a tool for directing further experimental studies on tablets' performance and an input for reactor design.

2. Theoretical background

A salt tablet comprises of two scales of interest: the μ m-size scale and the mm-size scale. We will refer to the μ m-size scale when we address properties of the powder particles, such as the intrinsic hydration kinetics of the salt. Tablets instead are mm-size samples, made of compressed powder particles and void space. The difference in structure at these two scales determines that their reaction kinetics will be dominated by a different kinetic parameter.

2.1. The µm-size scale: hydration kinetics of salt powders

The hydration of salt powders can be described by the conversion X, which goes from 0, fully anhydrous salt or low hydrate phase, to 1, higher hydrate phase. The rate of hydration, dX/dt, depends on the intrinsic reaction constant k (s⁻¹) as described by [40]:

$$\frac{dX}{dt} = k \frac{v}{RT} \left(p_w - p_{eq} \right) \tag{1}$$

where T (K) is the temperature of hydration, R (J mol $^{-1}$ K $^{-1}$) is the gas constant, ν (m 3 mol $^{-1}$) is the volume of salt that reacts per mole of water and $\left(p_w-p_{eq}\right)$ (mbar) is the driving force. Here, p_w is the water vapor pressure in air and p_{eq} is the water vapor pressure of the hydration transition. The water vapor pressure at equilibrium at any temperature can be calculated from Clausius-Clapeyron equation [41] for a dehydration reaction [42] as

$$p_{eq} = p^{ref} exp\left(\frac{\Delta S}{R}\right) exp\left(-\frac{\Delta H}{RT}\right) \tag{2}$$

where p^{ref} is equal to 1 bar, ΔS (J mol⁻¹ K⁻¹) is the standard entropy of dehydration per mole of water and ΔH (kJ mol⁻¹) is the standard enthalpy of dehydration per moles of water. Despite we could have used other more accurate models to reproduce the hydration rate [36,37], based on previous experimental work [4,31,40,43] this is constant almost up to full conversion, therefore also a linear model can effectively provide an estimate for k. The only assumption made at this stage is that powder particles are not porous.

2.2. The mm-size scale: hydration kinetics of salt tablets

The hydration kinetics at the tablet scale can either be reaction limited or diffusion limited. The second Damköhler number, Da_{II} , can help to assess which of the two mechanisms is dominating [40]:

$$Da_{II} = \frac{L^2 k}{D_{eff}} \tag{3}$$

where L (mm) is the characteristic length of the system and D_{eff} (mm² s⁻¹) is the effective diffusion coefficient. Da_{II} is defined as the ratio of L^2/D_{eff} (s), the diffusion time scale, and 1/k, the powder reaction time scale. If $Da_{II} < 1$, the hydration is reaction limited, and the equation to describe the rate of water absorption is equal to Eq. (1). If $Da_{II} > 1$, the hydration is diffusion limited and based on [40] the rate of hydration is

defined as:

$$\frac{dX}{dt} = \gamma \frac{D_{eff}}{RT} \frac{\left(p_w - p_{eq}\right)}{L^2} \frac{1}{X} \tag{4}$$

Eq. (4) describes the movement of a hydrate phase front within a mm-size tablet powered by the diffusion of water vapor, as portraited in Fig. 1. The parameter γ (cm³ mol⁻¹) is defined in terms of the molecular mass, M_d (g mol⁻¹), and the bulk density, $\rho_c(1-\Phi_d)$ (g cm⁻³), of the anhydrous or lower hydrate phase and the total moles of water exchanged, b:

$$\gamma = \frac{M_d}{b\rho_c(1 - \Phi_d)} \tag{5}$$

Both Eqs. (4) and (5) assume that the volume variation of a tablet during hydration is small. The effective diffusion coefficient is a function of the diffusion coefficient of water vapor in air, D_{air} , the porosity, Φ_h , and the tortuosity, τ_h , of a tablet in the hydrated state:

$$D_{eff} = \frac{D_{air} \Phi_h}{\tau_h} \tag{6}$$

For the details of the derivation the reader is referred to [40].

2.3. Making power output predictions through a scaling factor

Eq. (4) describes the hydration rate of a salt tablet as regulated by the transport of water through its pores. This is dependent on the structure $(\varepsilon_h, \tau_h, L)$ as well as on the type of hydration reaction (through p_{eq}). Here we want to elaborate the role of the hydration reaction on the power output while keeping constant all characteristics regarding the structure.

The power, P (W), produced by a tablet is the product of the amount of water molecules diffusing through its surface, I (mol/s) and ΔH :

$$P = I \Delta H \tag{7}$$

The total transport of water vapor into the pores is given by the integral of \vec{J} (mol m²s⁻¹) over the surface A (m²) of the tablet exposed to water vapor:

$$I = \oint \overrightarrow{J} \cdot \overrightarrow{n} \, dA \tag{8}$$

where \overrightarrow{n} is a normal vector to the surface. The previous equation results into

$$I = - \oint \overrightarrow{n} \cdot D_{eff} \nabla c \, dA \tag{9}$$

by introducing Fick's law $\overrightarrow{J} = -D_{eff} \nabla c$, where c (mol m⁻³) is the

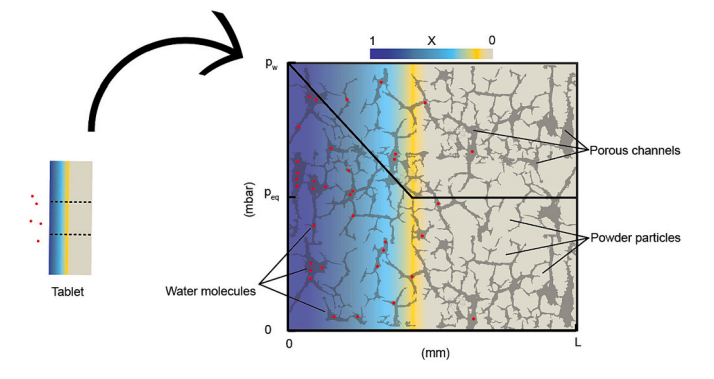


Fig. 1. Schematic of the interior of a tablet while hydrating according to a 1D diffusion description. The diffusion front moves along a characteristic distance, L, from left to right. The color gradient represents the degree of conversion, X, at that specific distance. The water vapor pressure changes from the exterior, p_w , to the interface where hydrate and anhydrate phases are in equilibrium, p_{eq} . Past this interface hydration does not take place.

concentration of water vapor in air. This equation can be expressed in terms of dimensionless parameters

$$\sigma \equiv \frac{A}{l^2} \tag{10}$$

$$\Psi \equiv \frac{c - c_{eq}}{c_w - c_{eq}} \tag{11}$$

$$\widehat{x} = \frac{x}{I}; \widehat{y} = \frac{y}{I}; \widehat{z} = \frac{z}{I}$$
 (12)

where l (m) is the diffusion length, c_w is the concentration of water vapor in air and c_{eq} is the concentration of water vapor in equilibrium at the hydration temperature. The obtained σ, ψ and $\widehat{x}, \widehat{y}, \widehat{z}$ are the dimensionless surface, concentration, and system coordinates, respectively. It follows that the next substitutions can be made for the concentration gradient and the tablet surface:

$$\nabla c = \frac{1}{l} \begin{pmatrix} d/d\widehat{x} \\ d/d\widehat{y} \\ d/d\widehat{z} \end{pmatrix} c = \frac{1}{l} \widehat{\nabla} c = \frac{c_w - c_{eq}}{l} \widehat{\nabla} \Psi$$
 (13)

$$dA = l^2 d\sigma (14)$$

After which, we obtain the following equation for *I*:

$$I = -D_{eff}(c_w - c_{eq})l \not \!\!\!\!/ \overrightarrow{n} \cdot \widehat{\nabla} \psi \, d\sigma \tag{15}$$

In this equation we distinguish two components. The first one is the driving force, c_w-c_{eq} , determined by the thermodynamics of the hydration transition of the salt type. The second one, $-D_{eff}l \oint \vec{n} \cdot \hat{\nabla} \psi \ d\sigma$, characterizes the vapor transport and its relation to the geometry and structure of the tablet. It follows from Eqs. (7) and (15) that the power output of geometrically identical tablets made from different salts varies with ΔH and c_w-c_{eq} :

$$P \propto \Delta H \left(c_w - c_{eq} \right) \tag{16}$$

This is rewritten in terms of water vapor pressure by applying the ideal gas law, and scaled with respect to the applied water vapor pressure, p_w :

$$P \propto \frac{\Delta H}{RT} \frac{\left(p_w - p_{eq}\right)}{p_{out}} \equiv \Lambda \tag{17}$$

From now we will refer to Λ (–) as a power scaling factor. By substitution of p_{eq} into (17) the final expression becomes:

$$\Lambda = \frac{\Delta H}{RTp_{w}} \left[p_{w} - p^{ref} exp\left(\frac{\Delta S}{R}\right) exp\left(-\frac{\Delta H}{RT}\right) \right]$$
 (18)

3. Materials and methods

3.1. Materials preparation and tablets manufacturing

Strontium bromide hexahydrate and calcium oxalate monohydrate powders are purchased from Alfa Aesar and Sigma Aldrich. SrBr $_2$ ·6H $_2$ O powder was milled (Fritsch planetary ball mill) and sieved to obtain a single fraction (50–164 µm). CaC $_4$ O $_4$ ·H $_2$ O powder was dehydrated in the oven at 160 °C and had a final particle size smaller than 10 µm as measured by scanning electron microscopy (SEM). Dehydration of this powder prior pressing was necessary as tablets pressed with CaC $_4$ O $_4$ ·H $_2$ O were not stable after dehydration. The powders were then mixed with 3 and 5 wt% of graphite (Graphterm 23-99,9) to facilitate pressing, respectively for CaC $_2$ O $_4$ and SrBr $_2$ ·6H $_2$ O. Cylindrical tablets were obtained using a column press (PO-Weber PW-40 2) in the range of

0.85 kbar and 8.5 kbar, Fig. 2. A mass of powder equal to 350 mg (SrBr $_2$ -6H $_2$ O) or ranging from 500 to 700 mg (CaC $_2$ O $_4$) was pressed for 30 s. The produced tablets had a diameter of 12.3 mm (SrBr $_2$ -6H $_2$ O) and 12.6 mm (CaC $_2$ O $_4$), and a thickness 1.4 \pm 0.1 mm (SrBr $_2$ -6H $_2$ O) and 4 \pm 0.1 mm (CaC $_2$ O $_4$), as measured by a caliper. The characteristics of the powders influenced the size and bulk density of the final product. SrBr $_2$ -6H $_2$ O powder contained more water and had a larger particle size, while CaC $_2$ O $_4$ powder was very dry and had a very small size. SrBr $_2$ -6H $_2$ O powder compacted very densely, because of the action of freed water and the fragmentation of the powder particles due to the compression. CaC $_2$ O $_4$ powder compacted less effectively due to the absence of free water and probably the presence of stronger interparticle forces that prevented the free flow of the powder particles. Table 1 summarizes the characteristics of each sample.

3.2. Thermogravimetric analysis (TGA)

The kinetic analysis on salt powders was performed on a Mettler Toledo TGA/DSC3+ instrument connected to a home-built humidifier. Powder samples with a weight of 4 to 6 mg were placed in an aluminum 40 μ l crucible. Once in the furnace they are flushed by a N₂ flow at 300 ml min. The humidifier moisturizes a fraction of the set flow according to the water vapor pressure (p_w) of choice. The wet and dry flow ratios were calibrated by detecting the deliquescence points of LiCl·H2O, MgCl₂·6H₂O and K₂CO₃·1.5H₂O at 25 °C [44]. The sample temperature was calibrated by determining the melting points of In, Pb and Zn standards through the heat flow signal under flow of N2. After the calibration, the accuracy on the p_w was 0.2 mbar. In a kinetic measurement, samples were first equilibrated at the conditions at which the lowest hydrate is the only phase present. SrBr₂·H₂O was obtained from SrBr₂·6H₂O at 60 °C and 1.7 mbar [43]. CaC₂O₄ was equilibrated at 160 °C and under pure nitrogen flow. This equilibration lasts as long as necessary to achieve a constant mass. After this first period, the temperature was switched to 21 °C at the maximum speed of the instrument (20 K min⁻¹). After 30 mins or when buoyancy effects have stabilized, the p_w was set to the desired value.

3.3. X-ray diffraction (XRD)

The phase composition of powder particles and millimeter tablets was checked by X-ray diffraction (XRD) and analyzed with the help of Rigaku PDXL2 software. The obtained diffractogram was then compared with references from the Crystallographic Open Database (COD). The instrument operated is a Rigaku Miniflex 600 X-ray diffractometer (Cu $K\alpha$ radiation; Be monochromator, $\lambda=1.5419$ Å, 40 kV, 15 mA) equipped with a D/tex Ultra2 1D detector. The milled powder and millimeter tablets were positioned in the instrument on top of a Nickel sample holder and the diffractograms are collected with a resolution of $0.05^{\rm o}$ and a speed of $5^{\rm o}$ min $^{-1}$. The diffractograms were taken after milling of the powder, after dehydration of the tablets in the oven. This was to ensure the presence of





Fig. 2. Tablets of SrBr₂·6H₂O (left) and CaC₂O₄ (right).

Table 1

Properties of the manufactured tablets resulting from the average of 4 samples. Samples are characterized by the manufacturing pressure applied to the powder mixture for 30 s, the density $(\Gamma_{as}=m/V\rho_c)$ (maximum standard deviation ± 1 %), the thickness (accuracy $=\pm 0.01$ mm) and the diameter (± 0.01 mm) of the tablets right after pressing.

| | Pressure (kbar) | Density (%) | Thickness (mm) | Diameter (mm) |
|--------------------------------------|--------------------|----------------|-------------------|------------------|
| SrBr ₂ ⋅6H ₂ O | 0.85 | 84.6 | 1.4 | 12.3 |
| | 5 | 91.5 | 1.3 | 12.3 |
| | 8.5 | 92 | 1.3 | 12.3 |
| CaC ₄ O ₄ | 0.85 | 49 | 4 | 12.6 |
| | 2.55 | 57 | 3.9 | 12.7 |
| | 6 | 66 | 3.8 | 12.7 |
| | 8.5 | 72 | 3.8 | 12.7 |

a single phase (SrBr $_2$ ·H $_2$ O or CaC $_2$ O $_4$) at the start of the hydration experiments. Tablets of CaC $_2$ O $_4$ were not analyzed in the XRD since they had to be dehydrated fully. The obtained results can be checked in the Appendix (Figs. A1 and A2).

3.4. Density and porosity measurements

The bulk density of a tablet was calculated by dividing its mass, m (mg), by its volume, V (mm 3). This value was then divided by the crystal density ρ_c (mg mm $^{-3}$) of the salt according to the specific hydration state to obtain Γ (–):

$$\Gamma = \frac{m}{V_O} \tag{19}$$

Since it is expressed relatively to the crystal density, Γ can be easily converted into porosity, Φ (–), which is a key parameter for understanding transport properties. A subscript accompanies Γ and Φ to indicate the state of the tablet: the as-prepared state, immediately after pressing, (Γ_{as} , Φ_{as}), after dehydration (Γ_d , Φ_d) or after hydration (Γ_h , Φ_h). The crystal densities of SrBr₂·6H₂O, SrBr₂·H₂O, CaC₂O₄ and CaC₄O₄·H₂O have been obtained respectively from [45–48]. The accessible porosity, instead, was determined by submersion of the tablets in hexadecane and by application of an under pressure of 9.3 kPa on the manometer. This method makes the trapped air in the pores escape and be substituted by the liquid, once the under pressure is lifted. The volume of the pores accessible to the solvent was obtained by measuring the difference in the tablet weight before and after submersion and diving the result by the density of the liquid. This procedure was repeated until no more air bubbles were seen emerging from the tablet.

3.5. Measuring conditions and methodology during the study of tablets' hydration

The tablets were dehydrated in the oven, either at 60 °C (SrBr₂·H₂O) or 160 °C (CaC2O4) to ensure that SrBr2 is in its monohydrate form and CaC2O4 is anhydrous. After two days, the weight measured corresponded to the theoretical weight of the tablet in the lowest hydrate phase. All hydration measurements were then performed at room temperature and constant humidity, which was obtained by preparing a saturated salt solution in a closed desiccator that produced a welldefined relative humidity (RH) of 85 %, 65 %, 53 %, 43 %, 33 % and 22 %, respectively in case of a KCl, NaNO₃, Mg(NO₃)₂, K₂CO₃, MgCl₂ and CH₃COOK solution [44]. The homogeneity of water vapor in the desiccator was ensured by a small ventilator. The weight of the tablets was measured on a Mettler Toledo analytical balance. The tablet was quickly taken out of the desiccator, weighted, and then placed back. The hydration kinetics were examined with respect to the water vapor pressure and the porosity of the tablets. The tablets used in the same test had an equal thickness, so that the contribution to hydration from water vapor diffusion through the side walls was equal in all cases. The side walls

influence on the hydration rate is described in Fig. A6 and A7 of the Appendix for both salts. The diffusion coefficients associated with CaC_2O_4 hydration were obtained from measurements performed on sealed tablets (Fig. A8), so that the hydration could be considered truly 1-dimensional.

4. Results and discussion

This section starts with the structural characterization of mm-size tablets. We are going to show how the volume and porosity vary during the different measurement phases. The second section focuses on the TGA measurements performed on μ m-size powder from which the hydration reaction constant, k, is extracted. In Section 4.3 we report on the gravimetric analysis of the hydration kinetics of tablets, where we have distinguished in between the role of the driving force and the role of the structure (volume, porosity). From these measurements we have obtained the D_{eff} coefficients as a function of the porosity. Based on these two parameters, we have calculated the second Damköhler number to identify the validity domain of each hydration mechanism, either intrinsic kinetic controlled or diffusion controlled, as explained in the theory section. Finally, in Section 4.4, we use the diffusion limited model to calculate a power scaling factor that allows us to predict and compare the power performance of many different salts.

4.1. Structure of the mm-size tablets before and after hydration

As the hydration kinetics of tablets may depend on their size and structure, the evolution of volume and porosity was monitored after sample preparation, after dehydration and after one hydration cycle. The amount of mass used to produce $SrBr_2\cdot 6H_2O$ tablets was always the same, instead the amount of mass used of CaC_2O_4 increased with the manufacturing pressure to obtain an equal thickness (3.8 mm, Table 1). The volume was calculated from the measured diameter and thickness, while the porosity, Φ , is obtained from the density, Γ , calculated according to Eq. (19).

The volume of the tablets is plotted in Fig. 3(a) and (b) with respect to the manufacturing pressure. Each data point is obtained by averaging the volume of at least four samples prepared in the same way. The standard deviation is substantially larger in the re-hydrated tablet groups compared to the others either because of slight deformations (SrBr₂) or brittleness (CaC₂O₄). In the case of SrBr₂, the volume after preparation decreased with the manufacturing pressure, from 167 to

152 mm³ (Fig. 3(a), black squares). However, the variation in thickness was at most 0.1 mm. This trend was still present after dehydration (red squares), but not anymore after re-hydration (blue squares). The tablets after dehydration shrank with respect to the state after pressing (151–139 mm³), but re-expanded after hydration, by at most 30 mm³ (\sim 19 %).

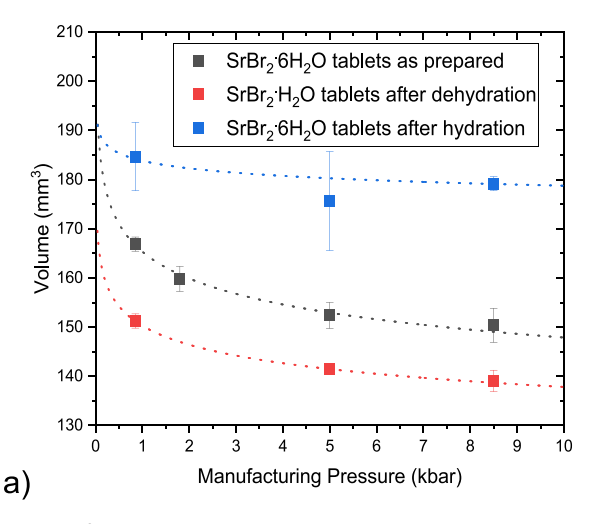
In the case of CaC_2O_4 the volume was measured only for two sets of samples as the tablets have been pressed from the anhydrous phase (Fig. 3(b)). The volume did not vary significantly with the manufacturing pressure and the expansion after hydration was about 100 mm^3 (~ 20 %) at all manufacturing pressures.

The volume expansion of salts due to hydration is a well-known fact [49]. In view of thermochemical energy storage it was recently documented for K_2CO_3 powder particles by Beving et al. [29]. Moreover, that tablets decrease in volume after dehydration was described as well by Aarts et al. for K_2CO_3 [40]. In the case of $SrBr_2\cdot H_2O$ hydration the volumetric expansion is significantly smaller than the expansion expected from theoretical calculations (+113 %). On the contrary, CaC_2O_4 should expand by <1 %. Phenomena such as pore filling and loss of intraparticle cohesiveness could explain these discrepancies.

The porosity has been calculated and plotted as a function of the manufacturing pressure in Fig. 4(a) and (b), respectively for SrBr $_2$ and CaC $_2$ O $_4$. The porosity of SrBr $_2$ -6H $_2$ O tablets was low (<15 %) and varied with the manufacturing pressure from 8 to 15 %. Once water was lost due to dehydration, the porosity increased to 55 %. After rehydration the porosity was larger with respect to the start because the tablets expanded, but it decreased with respect to the dehydrated state. On the contrary, the porosity of CaC $_2$ O $_4$ tablets was very high right after pressing and it varied substantially as a function of the manufacturing pressure s (53 % to 27 %) because of the increase in mass (see Materials and methods). As before, the porosity in the hydrated state was larger than in the initial state.

To describe the internal structure of mm-size tablets we need to distinguish in between total porosity and accessible porosity. Therefore, we also studied the internal structure of tablets by liquid impregnation.

The accessible porosity was measured by impregnation of the tablets by hexadecane. The results are plotted against the total porosity calculated from the mass and the geometric volume in Fig. 5. Each data point refers to a single sample. The accessible porosity of as-prepared $SrBr_2\cdot 6H_2O$ tablets (black squares) varied from 0 % to 12 % as the total porosity varied in between 11 % and 16 %. After dehydration (red squares) the accessible and total porosity were not significantly



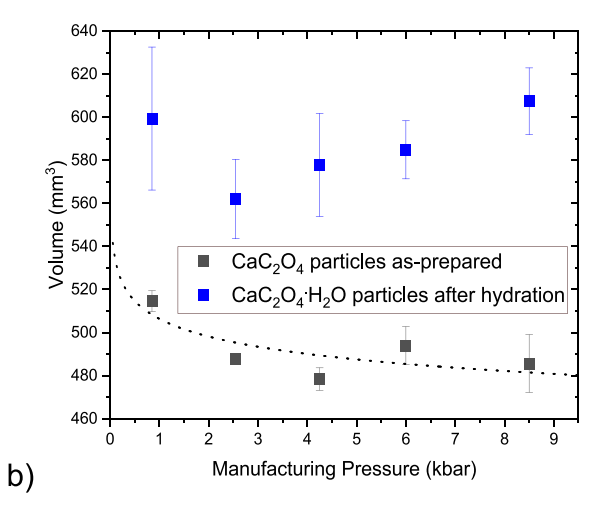


Fig. 3. Volume (mm³) of tablets as a function of the manufacturing pressure (kbar), in (a) for $SrBr_2$ and in (b) for CaC_2O_4 . The black symbols represent the tablets right after pressing, the red symbols the same tablets after dehydration, the blue symbols the tablets after hydration. The error bar is a standard deviation. The legend reports for each data set the phase composition of the tablets. Note that the as-prepared phase for $SrBr_2$ is the hexahydrate, while for CaC_2O_4 is the anhydrous. For CaC_2O_4 tablets the amount of mass was increased with the manufacturing pressure in order to have an equal thickness. (For interpretation of the references to color in this figure legend, the reader is referred to the web version of this article.)

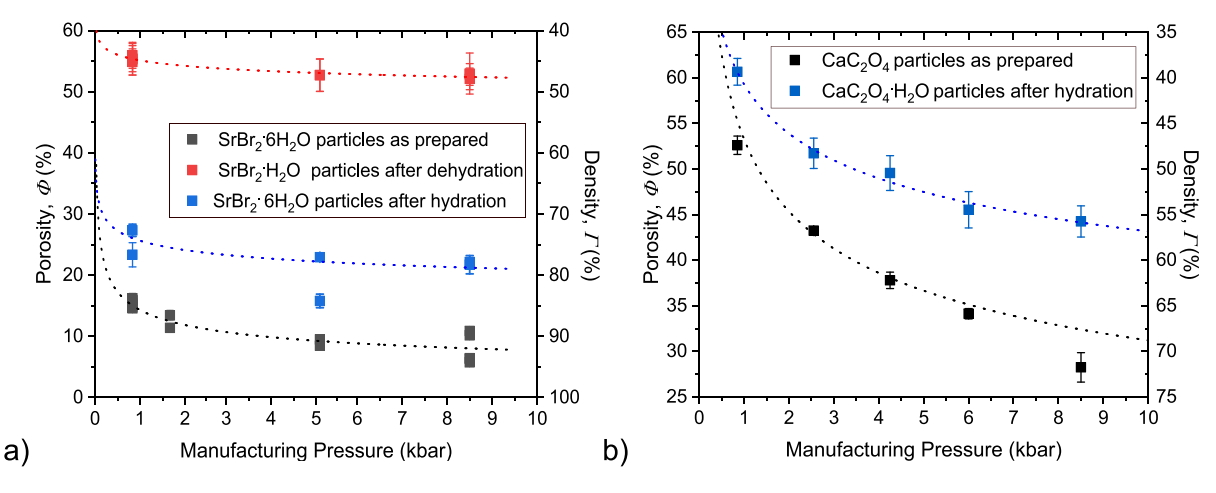


Fig. 4. Porosity (%) of tablets as a function of the manufacturing pressure (kbar), in (a) for $SrBr_2$ and in (b) for CaC_2O_4 . The black symbols represent the tablets right after pressing, the red symbols the same tablets after dehydration, the blue symbols the tablets after hydration. The error bar is a standard deviation. The legend reports for each data set the phase composition of the tablets. Note that the as-prepared phase for SrB_2 is the hexahydrate, while for CaC_2O_4 is the anhydrous. (For interpretation of the references to color in this figure legend, the reader is referred to the web version of this article.)

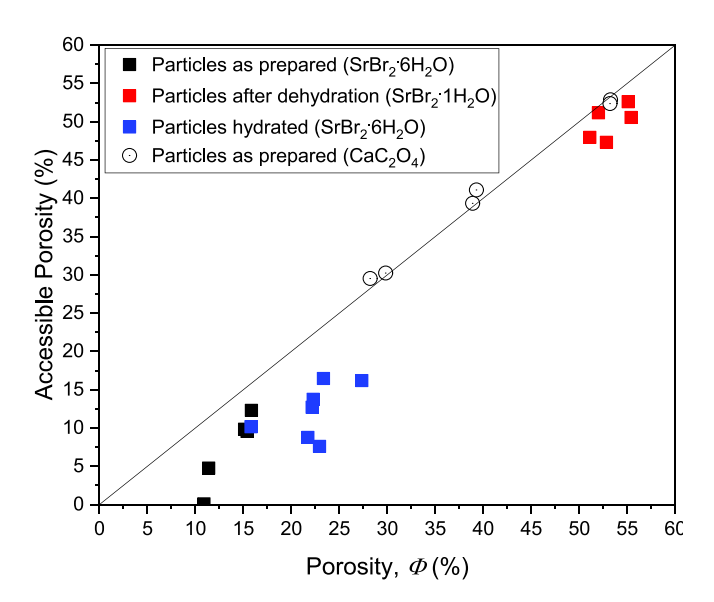


Fig. 5. The accessible porosity (%), measured by hexadecane impregnation, with respect to the porosity, Φ (%), obtained from the crystal density of the salt and the measurements of the mass and the geometric volume of the tablet. Each data point is a sample. The accessible porosity has been measured for asprepared samples, dehydrated and re-hydrated, which correspond respectively to black, red and blue data points. Squares are assigned to $SrBr_2$ while circles to CaC_2O_4 . The accessible and total porosity are equal on the line. The total porosity increases as the manufacturing pressure decreases. (For interpretation of the references to color in this figure legend, the reader is referred to the web version of this article.)

different. In the re-hydrated tablets (blue squares), the accessible porosity increased from 8 % to 15 % as the total porosity varied from 15 % to 27 %. In general, the accessible porosity increased at each stage with respect to the as-prepared state. It is always smaller than the corresponding total porosity, since all data points fall under the line. However, the data points on the dehydrated and re-hydrate samples fall mush closer to the line, indicating an increased accessibility of the tablet as the total porosity increases. CaC_2O_4 tablets could be fully impregnated without using an under pressure. The accessible porosity in these tablets (black open circles) was exactly equal to the porosity measured geometrically. Although CaC_2O_4 monohydrate tablets could not be measured with this method, their interconnectivity is also likely to be

very large, since they had a very large porosity (Fig. 4(b)).

4.2. The μ m-size scale: hydration kinetics of powder particles

The hydration kinetics of the salts are first measured in absence of transport limitations. This is possible by thermal gravimetric measurements of small amounts of powder particles under controlled temperature (21 $^{\circ}$ C) and water vapor pressure. The intrinsic reaction constant, k, was obtained from these measurements by calculating the first derivative of the reaction conversion curve and applying Eq. (1). The TGA measurements are reported in the Appendix (Fig. A5) while the intrinsic kinetic constant is plotted in Fig. 6 with respect to the driving force.

In the case of $SrBr_2 \cdot H_2O$ (Fig. A5, left) the k parameter was obtained from the first derivative calculated at half conversion, X=0.5, corresponding to 2.5 mol of water per mol of salt. In fact, we found that a linear fit reproduced accurately the hydration kinetics of $SrBr_2 \cdot H_2O$ up to at least 50 % conversion, as visible in Fig. A5. The resulting k, as shown in Fig. 6, did not vary in this water vapor pressure range,

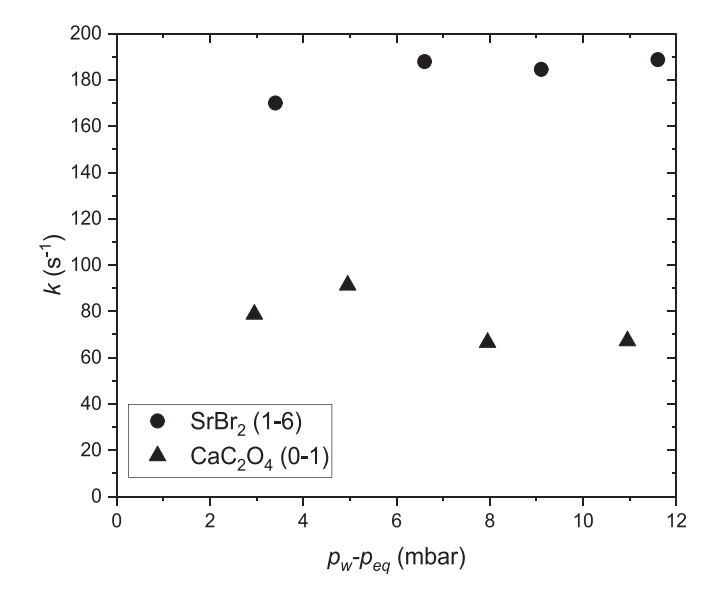


Fig. 6. Hydration kinetic constant, k (s^{-1}), at half conversion of SrBr₂·H₂O (circles) and at 0.3 mol mol⁻¹ of CaC₂O₄ (triangles), obtained from Eq. (1) and plotted as a function of the driving force, $p_w - p_{eq}$. The hydration curves have been measured at several water vapor pressures and 21 °C.

therefore justifying the model used. In the case of CaC_2O_4 hydration (Fig. A5), the first derivative was instead calculated at 0.3 mol of water per mol of salt and the found k values also did not show significant variation with the water vapor pressure. A subplot of Fig. A5 shows that the hydration rate is constant for all curves up to 0.3 mol mol⁻¹ and that a linear fit reproduces the curve satisfactory, with the largest deviation being at 11 mbar.

A prediction of the Da_{II} can be made based on the found values for k. The diffusion coefficient can take values in between 0 and 24.9 mm²s $^{-1}$, which is the diffusion coefficient of water vapor in air [50]. In literature, for example, we found that $D_{eff}=0.72~{\rm mm}^2{\rm s}^{-1}$ at 25 °C for sandstone when $\varepsilon=16.8\%$ [51] and $D_{eff}=3.1~{\rm mm}^2{\rm s}^{-1}$ at 20 °C for soil when $\varepsilon=64\%$ [52]. Therefore, the Da_{II} calculated using Eq. (3) for respectively SrBr2 and CaC2O4 1 mm tablets and taking $D_{eff}=2~{\rm mm}^2{\rm s}^{-1}$ are $Da_{II}=92.5~{\rm and}~Da_{II}=40$. Since in both cases $Da_{II}>>1$, it is justified to expect that the hydration of tablets presented in the following sections could be diffusion limited.

4.3. The mm-size scale: hydration kinetics of tablets

To establish whether the hydration kinetics of tablets are diffusion limited or not, we must measure the hydration rate as a function of the driving force and the structure. These tablets were produced by compression, hydrated inside a desiccator at room temperature and their weight was measured on an analytical balance. First, we discuss the hydration of identical tablets under varying driving force. Afterwards, we discuss how the hydration rate depends on the structure of the tablets. Finally, we apply Eq. (5) and evaluate the validity of the diffusion limited model for SrBr2 and CaC2O4 hydration.

4.3.1. The hydration of mm-size tablets: the role of the driving force The dependency of the hydration kinetics on the driving force was

tested by hydrating geometrically identical mm-size tablets at room temperature and controlled humidity. The tablets were identical because they had been manufactured at the same pressure (0.85 kbar) starting from the same mass, having an average as-prepared porosity of 15.5 % and 53 %, respectively for $SrBr_2 \cdot 6H_2O$ and CaC_2O_4 .

The position of the measurement points with respect to the metastable and the phase lines are summarized by the light blue points in Figs. A3 and A4 of the Appendix. The measurement conditions were out of the metastable zone of each hydration reaction and below the deliquescence line of the highest hydrate. The hydration curves are plotted in Fig. 7(a) and (b), respectively for SrBr₂·H₂O and CaC₂O₄. The water uptake is plotted as loading - moles of water over moles of salt hydrate and varies from 1 to 6 for SrBr₂·H₂O and for 0 to 1 for CaC₂O₄. The data points up to half conversion are fitted by a square root of time function, as this is the solution to Eq. (4). Half conversion was selected as a common threshold for fitting because the moment of full conversion could not always be measured precisely. In this way the influence of end effects was excluded from the fitting. The reaction rate of SrBr₂·H₂O hydration increased as the RH changed from 22 % to 53 %. The same was observed for CaC2O4, in which case the RH was varied from 7 % to 33 %. Comparing with powder hydration, Fig. A5, in all cases the hydration is slower on the tablet scale, which one might expect if diffusion limits the reaction. In the Theoretical background section, we have introduced that the hydration rate is proportional to $p_w - p_{eq}$, according to Eq. (4). This was also found when calculating the power output and excluding the influence of the structure, as in Eq. (17). Consequently, the hydration curves of tablets identical in shape, size and structure will fall onto a single master curve if the loading is plotted as a function of $\Delta p t$. This operation is performed in Fig. 7(c) and (d) and resulted in the curves overlapping with each other. We conclude that the hydration of tablets made of SrBr2·H2O and CaC2O4 agrees with the driving force expected from the theory of a diffusion limited hydration and that this is

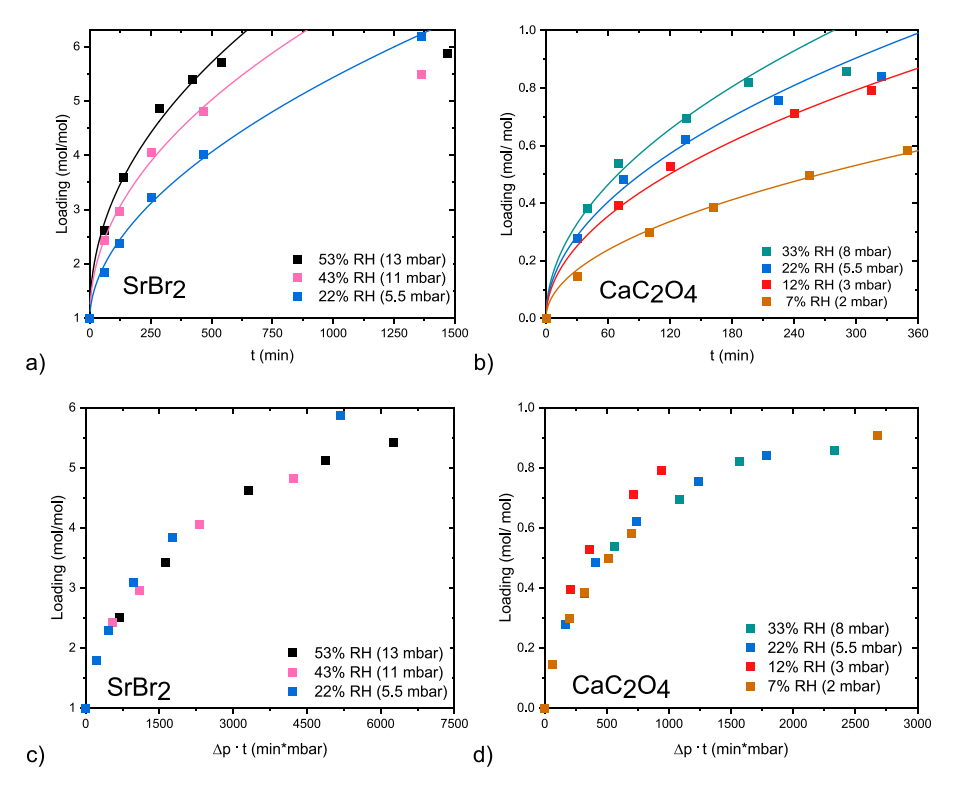


Fig. 7. (a) Hydration loading curves as a function of time of $SrBr_2 \cdot 6H_2O$ tablets pressed at 0.85 kbar, dehydrated and then hydrated at 21 °C in desiccators kept at a different relative humidity. The average porosity of these tablets as-prepared is 15.5 %; (b) Hydration loading curves as a function of time of CaC_2O_4 tablets pressed at 0.85 kbar and hydrated at 21 °C in desiccators kept at a different relative humidity. The average porosity of these tablets as-prepared is 53 %; (c and d) the same loading curves are here represented against time scaled by the driving force $(p_w - p_{eq})$. In all plots, symbols represent experimental data, while solid lines are obtained from a square root of time fit of the data points up to half conversion. Tablets used in each set have the same dimensions.

why the time scales of tablets' hydration are longer than the time scales of powder particles.

4.3.2. The hydration of mm-size tablets: the role of the structure

After the driving force, the structure is the additional factor that may influence the hydration kinetics of mm-size tablets. In this section we are going to show the results on the hydration of mm-size tablets as a function of the porosity. This is investigated by measuring a set of three tablets pressed at increasing manufacturing pressure as they hydrate under controlled temperature and humidity inside a desiccator. The tablets within each set have the same dimensions, as described in the Materials and method section.

In Fig. 8, the mass uptake in time of each sample is represented by the number of moles of water absorbed relatively to the total moles of the anhydrous salt (SrBr $_2$, CaC $_2$ O $_4$). In Fig. 8(a), SrBr $_2$ ·H $_2$ O tablets are hydrated at 53 % RH. The tablet of 16 % porosity hydrated at a faster rate than the tablets of 9 % and 6 % porosity. An equal accessible porosity in the re-hydrated state may explain why these last two curves overlapped. In Fig. 8(b), CaC $_2$ O $_4$ tablets are hydrated at 33 % RH. Again, the hydration rate increased with the porosity. The calculation of the effective diffusion coefficients should result into an equivalent dependency from the porosity. These diffusion coefficients are extracted from the hydration measurements of tablets by fitting the curves with the analytical solution of Eq. (4).

The diffusion coefficients obtained in this work are plotted in Fig. 9 together with data points obtained from [40] on K_2CO_3 , as a function the density (porosity) of the hydrated tablets. Each data point is a measurement point. The values obtained from the mathematical fit are in close agreement with the literature results. In fact, when the density of the hydrated tablets decreased, moving from K_2CO_3 , to $SrBr_2$ and to CaC_2O_4 , the diffusion coefficients increased. Apart from some stochasticity, the data points all together depicted a master curve and a monotonous increase of D_{eff} with the porosity, in line with Eq. (6). At last, from the values for k and D_{eff} the Second Damköhler number, Da_{II} , could be calculated using Eq. (3). The values found (Table 2) are always much larger than one for all samples, indicating that the hydration of mm-size tablets of $SrBr_2 \cdot H_2O$ and CaC_2O_4 is indeed dominated by diffusion of water vapor and not by intrinsic reaction at the μ m-size particle scale.

4.3.3. Hydration of mm-size tablets of any salt is diffusion limited

The data presented in the last three sections supported the idea of a front diffusion limited hydration in case of mm-size tablets. The hydration kinetics of the studied tablets increased with the relative humidity and with the porosity. We showed that the driving force can be indeed represented by Δp , and through the model we found that the

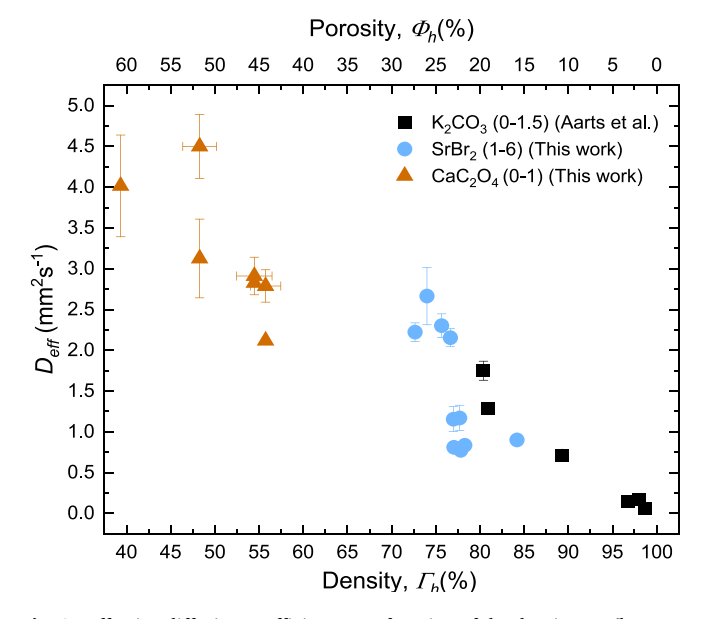


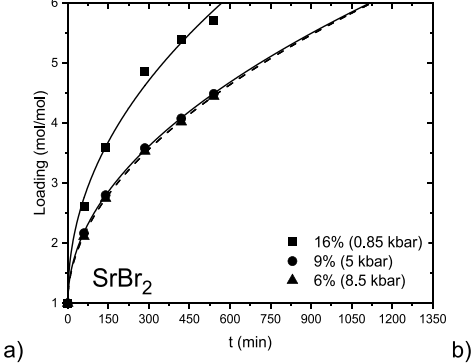
Fig. 9. Effective diffusion coefficients as a function of the density, Γ_h (lower X-axis), or porosity Φ_h (upper X-axis), of fully converted tablets. A different symbol is assigned to every reaction as reported in the legend. The circles and triangles are data points obtained in this work from measurements performed at different humidity conditions. The squares are reproduced from reference [40] and come from measurements performed on tablets compressed from 50 to 164 μ m powder size distribution and hydrated at 33 % RH and RT.

Table 2 Second Damkhöler numbers calculated for $SrBr_2 \cdot H_2O$ and CaC_2O_4 tablets according to the manufacturing pressure. The Da_{II} was calculated using values of k measured at 13.2 mbar and 5.5 mbar for $SrBr_2$ and CaC_2O_4 , respectively. The thickness (L, mm) and porosity of the tablets as-prepared (Γ_{as} ,%) are also reported to ease the identification of the sample.

| | 0.85/ | 0.85/2.55 kbar | | 4.5/5 kbar | | | 8.5 kbar | | |
|--|------------|----------------|------------|-------------|------------|------------|-------------|------------|------------|
| | L | Γ_h | Da_{II} | L | Γ_h | Da_{II} | L | Γ_h | Da_{II} |
| SrBr ₂ CaC ₂ O ₄ | 1.4 3.9 | 15.4 53 | 158 325 | 1.28 3.8 | 8.5 34 | 137 520 | 1.26 3.8 | 8 28 | 317 618 |

resulting D_{eff} depended on the porosity and fell in an interval expected for diffusion of water vapor in pores. We can now discuss which values Da_{II} takes in a wider list of reactions, using constants k and D_{eff} obtained so far to define its range.

Fig. 10 displays the result of this estimate for two values of $L:100~\mu m$



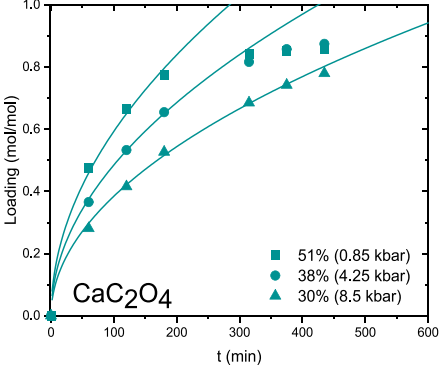


Fig. 8. Hydration loading curves as a function of time obtained from mm-size tablets pressed with increasing manufacturing pressures (0.85, 4.25, 5 and 8.5 kbar) and then hydrated at room temperature and (a) 53 % RH, $SrBr_2$ · H_2O or (b) 33 % RH, CaC_2O_4 . Symbols represent different manufacturing pressures. Each line results from a square root of time fit of the data points up to half conversion. The values in the legend are the porosity of the tablets right after pressing, therefore when the phases are $SrBr_2$ · GH_2O and CaC_2O_4 .

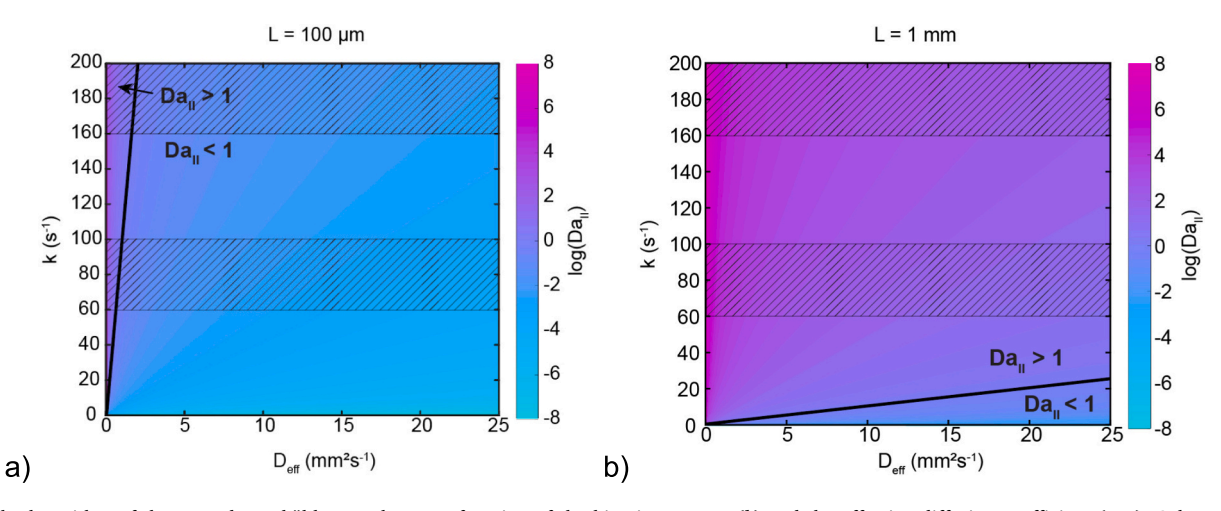


Fig. 10. The logarithm of the second Damköhler number as a function of the kinetic constant (k) and the effective diffusion coefficient (D_{eff}). Color map (a) is calculated for L = 100 μm, while color map (b) for L = 1 mm. The black line represents the place of points where $Da_{II} = 1$. Above the black line, $Da_{II} > 1$, the hydration kinetics are diffusion limited, below, $Da_{II} < 1$, reaction limited. The two stroked bands are placed to emphasize the interval of k found for SrBr₂ monohydrate (160 < k < 200 s⁻¹) and CaC₂O₄ hydration (60 < k < 100 s⁻¹).

(a) and 1 mm (b). Here the constant k varies from 0 s⁻¹ up to 200 s⁻¹ and D_{eff} spans from 0 to 24.9 mm²s⁻¹. The transition in between the reaction limited and diffusion limited regimes is emphasized by a straight black line, which represents the conditions where $Da_{II}=1$. When $Da_{II}<1$, hydration is dominated by the intrinsic kinetics of the powder particles. When $Da_{II}>1$, water diffusion is the limiting process. We see that when the distance to travel is small ($L=100~\mu m$), water diffusion is not limiting the hydration kinetics, except for extremely low values of D_{eff} . When the distance increases the opposite occurs. At this point, the hydration reaction may be still reaction limited only if k is extremely small. We conclude that the probability that the hydration of a mm-sized tablet is reaction limited is low.

4.4. Comparison of power scaling factors assuming the diffusion limit

Given the diffusion limited hydration, the power output of a tablet will depend on the driving force and on the structure (geometry, porosity and tortuosity). The salt type mainly influences the driving force if tablets with identical internal structure can be made. Therefore, we can classify salt hydration reactions based on the power output by calculating the previously introduced power scaling factor, Λ . Here Λ was calculated at $p_w=12$ mbar – which is the saturation water vapor pressure above a water source at 10 °C – and T=40 °C – which is desirable for space heating. Values are listed in Table 3 for those same reactions that have been introduced at the start, as well as for some reactions that have not been widely considered so far, but have an interesting value of Λ , like MnBr₂ and Ba(OH)₂. Each of these reactions involves one reaction step only. A more comprehensive view of Λ is shown by the color map in Fig. 11.

Fig. 11 shows all the hydration reactions in the database of Donkers

et al. [6] organized by their enthalpy and entropy of reaction, whose distribution is emphasized by the histograms along the x and y directions, respectively. The enthalpy interval is limited to the region with the maximum density of data points. The entropy interval instead has a lower boundary at $100 \, \mathrm{J} \, \mathrm{mol}^{-1} \, \mathrm{K}^{-1}$, which is the entropy of vaporization of water, and it is symmetrical with respect to $146 \, \mathrm{J} \, \mathrm{mol}^{-1} \, \mathrm{K}^{-1}$, were most of the data points fall. This feature of the distribution was already observed by Glasser et al. [53]. In fact, the entropy of reaction is often approximated by the entropy of sublimation of water in absence of a calculated or measured value and in [53] this was justified by the larger contribution to the entropy change given by water sublimation compared to the two solid phases. Each data point is characterized by a color according to its value of Λ , which varies from 0 (black) to 30 (orange). Higher values of Λ indicate a higher relative power output. The hydration reactions from Table 3 are labelled in the color map.

The black data points ($\Lambda \leq 0$) indicate reactions that cannot occur at the desired conditions. This occurred when $p_{eq} < 12$ mbar, because at this point the reaction is thermodynamically forbidden, since the driving force is smaller than 0 ($p_w - p_{eq} < 0$). We found that $SrCl_2(2-6)$ fell in this region. Colored data points ($\Lambda > 0$), on the other hand, indicate reactions that are thermodynamically allowed ($p_w - p_{eq} > 0$). These reactions also showed large variations in its value, depending on their enthalpy and entropy.

 Λ increases with the enthalpy. It increases 6 times in between $SrBr_2(1-6)$ and $SrCl_2(2-6)$ and 1.7 time in between $CaC_2O_4(0-1)$ and $MgCl_2(2-6)$. When comparing different transitions of the same salt, there may be large differences as well, as in between $SrCl_2$ (2–6) and (0–1), or $MgCl_2(4-6)$ and (0–1).

 \varLambda also increases when the entropy decreases. For example, \varLambda increases 3 times going from SrBr₂(1–6) to Ba(OH)₂(0–1). This aspect can

Table 3 Standard enthalpy (ΔH , (kJ mol⁻¹)) and standard entropy (ΔS , (kJ mol⁻¹ K⁻¹)) of dehydration of specific salt-water hydration transitions found in literature [6] and the respective equilibrium water vapor pressure (p_{eq}) and power scaling factor (Λ) at 40 °C.

| | MnBr ₂ (0–1) | CaC ₂ O ₄ (0-1) | K ₂ CO ₃ (0–1.5) | Na ₂ S (2–5) | Ba(OH) ₂ (0–1) | MgCl ₂ (4–6) | SrBr ₂ (1–6) | SrCl ₂ (2–6) |
|---|----------------------------|--|--|----------------------------|------------------------------|----------------------------|----------------------------|----------------------------|
| ΔH (kJ mol ⁻¹) | 76 | 69.5 | 65.8 | 62,9 | 56.1 | 58.2 | 56.5 | 53.7 |
| ΔS (J mol ⁻¹ K ⁻¹) | 163 | 134 | 156 | 149 | 127 | 138 | 141 | 143 |
| $p_{eq}(40 ^{\circ}\text{C})$ (mbar) | 0.07 | 0.03 | 3.11 | 1.98 | 1.91 | 3.21 | 8.84 | 32.43 |
| Λ(40 °C) (−) | 29 | 27 | 22 | 20 | 18 | 16 | 6 | -35 |

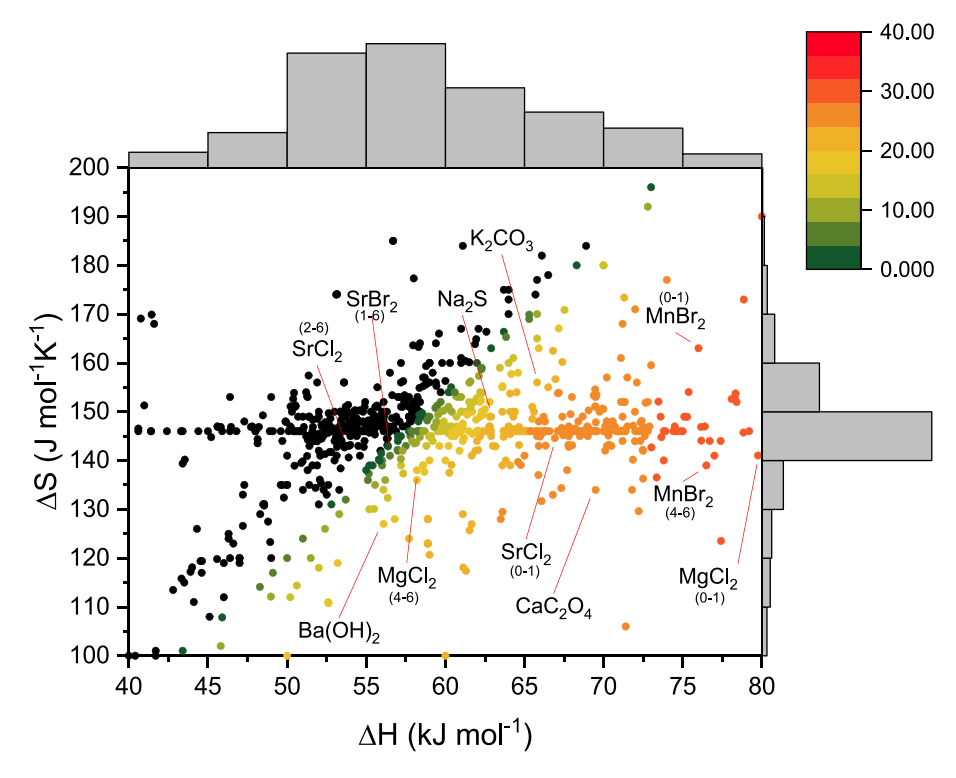


Fig. 11. The power scaling factor Λ at 40 °C and 12 mbar as a function of the entropy, ΔS , and enthalpy, ΔH , of reaction for all hydration reactions found in the database of Donkers et al. [6] The scaling factor changes from 0 (black dots) to 45 (red dots). The labelled data points are reported in Table 3. (For interpretation of the references to color in this figure legend, the reader is referred to the web version of this article.)

be related to the degrees of freedom the water molecules possess into the salt hydrate structure. When the entropy change is lower, the water molecules can adopt more configurations. One example is represented by CaC_2O_4 , which has a relatively low standard entropy. According to [48] the structure of CaC_2O_4 anhydrous is characterized by molecular channels which are filled by water molecules during hydration to give CaC_2O_4 monohydrate [47]. Since water molecules are accommodated in these channels, we also found that CaC_2O_4 anhydrous has a lower crystalline density (1.97 g cm $^{-3}$) [48] than in the monohydrate state (2.26 g cm $^{-3}$) [47], unlike most other salts [6].

5. Conclusion and outlook

In this work we have applied the recent hypothesis [40] that the hydration of mm-size salt tablets is diffusion limited to the study of the hydration behavior during the first cycle of two promising salt hydrates for thermochemical energy storage: $SrBr_2 \cdot H_2O$ and CaC_2O_4 .

The hydration kinetics of tablets made of both salts was dependent on the porosity and on the driving force. The values of D_{eff} obtained through the application of the diffusion model depend on the density of the tablets and not on the material. In fact, our results are in agreement with previous findings and with the literature on diffusion of water vapor in porous media. In the end, the estimation of the second Damköhler number based on k and D_{eff} confirmed that a hydration front must develop within the tablets.

The current findings established a domain of interests in which several combinations of k and D_{eff} resulted in the second Damköhler number being larger than 1. This implied the extension of the diffusion limited hydration hypothesis to a wider range of hydration reactions. Therefore the hydration of any mm-sized salt tablet is probably going to be limited by the formation and movement of a diffusion front through its length.

Consequently, the power output of a salt tablet is limited both by structural aspects and by the driving force. Since the importance of the salt selection resides in the driving force only, we compared the hydration kinetics of identical tablets of any shape and size by calculating the power output in the form of a scaling factor, Λ . This scaling factor depended on thermodynamic quantities (enthalpy and entropy) and temperature. We observed first that higher power factors were found for reactions with higher enthalpy (>60 kJ mol^-1) and lower entropy change (<146 J mol^-1 K^-1). Second, due to the statistical distribution of enthalpies and entropies, the spread in power scaling factor was between 0 and 30, at a defined temperature and water vapor pressure. Therefore, salt selection based on the tuning of the driving force, can potentially be very beneficial. In these terms the power scaling factor should be used complementary to the energy density as a parameter for discrimination.

In view of a higher power output, tablets suitable for a heat storage bed should figure among those with a high enthalpy. However, high enthalpies also signify higher equilibrium temperatures ($T>100\,^{\circ}\text{C}$) (Fig. A9), therefore a high temperature source is also necessary for the dehydration of these tablets. In the case of a low temperature application, it is instead important to choose hydration reactions which have a lower entropy change. For a new re-evaluation of the number of best salt candidates, it would be useful to investigate what material properties are responsible for this lower entropy change. One of these may be the presence of water molecules characterized by higher degrees of freedom in their motion once in the salt hydrate structure, as in the case of CaC₂O₄. The molecular structure of CaC₂O₄ is indeed characterized by zeolite-like molecular channels.

With respect to the methods used to increase the hydration rate of a mm-size tablet, this work highlights that the power output of tablets could only be increased by changing the structure of the material and not by increasing the intrinsic reaction rate. In this regard, it is also important to understand how the structure of these particles evolves during cycling and evaluate the presence of diffusion limitations even after several cycles. Once the mechanism is understood, related strategies could either envision ways to stabilize the evolving particle or to

develop methods to fabricate tablets highly porous but stable from the start. For those salts whose Damkhöler number is very close to 1, these developments could determine the occurrence of reaction limited mmsize particles. The diffusion limitation could also be overcome by accelerating the water transport into the tablet – for example by condensation and evaporation of water within the pores of the tablet—but this possibility has not been explored yet to the knowledge of the authors. Otherwise, it is only possible to avoid diffusion limited hydration by producing particles well below the mm-scale.

Funding

This project has received funding from the European Union's Horizon 2020 research and innovation program under grant agreement No 869810. This work reflects only the author's view. The European Commission is not responsible for any use that may be made of this information.

CRediT authorship contribution statement

Martina Cotti: Writing – original draft, Methodology, Investigation, Formal analysis, Conceptualization. Hartmut Fischer: Writing – review & editing, Supervision, Methodology, Investigation, Conceptualization. Olaf Adan: Writing – review & editing, Supervision, Methodology, Investigation, Funding acquisition, Conceptualization. Henk Huinink: Writing – review & editing, Supervision, Resources, Project administration, Methodology, Investigation, Funding acquisition, Conceptualization.

Declaration of competing interest

The authors declare that they have no known competing financial interests or personal relationships that could have appeared to influence the work reported in this paper.

Data availability

Data will be made available on request.

Acknowledgements

The authors would like to thank Hans Dalderop for his technical support and Joey Aarts for the rich discussions on tablets hydration.

Appendix A. Supplementary data

Supplementary data to this article can be found online at https://doi.org/10.1016/j.est.2024.111395.

References

- Energy, Transport and Environment Statistics, 2020 edition, European Union, Luxembourg, 2020.
- [2] S. Koohi-Fayegh, M.A. Rosen, A review of energy storage types, applications and recent developments, J. Energy Storage 27 (Feb. 2020) 101047, https://doi.org/ 10.1016/j.est.2019.101047.
- [3] M. Richter, E.-M. Habermann, E. Siebecke, M. Linder, A systematic screening of salt hydrates as materials for a thermochemical heat transformer, Thermochim. Acta 659 (Jan. 2018) 136–150, https://doi.org/10.1016/j.tca.2017.06.011.
- [4] S. Afflerbach, R. Trettin, A systematic screening approach for new materials for thermochemical energy storage and conversion based on the Strunz mineral classification system, Thermochim. Acta 674 (Apr. 2019) 82–94, https://doi.org/ 10.1016/j.tca.2019.02.010.
- [5] K.E. N'Tsoukpoe, T. Schmidt, H.U. Rammelberg, B.A. Watts, W.K.L. Ruck, A systematic multi-step screening of numerous salt hydrates for low temperature thermochemical energy storage, Appl. Energy 124 (Jul. 2014) 1–16, https://doi. org/10.1016/j.apenergy.2014.02.053.
- [6] P.A.J. Donkers, L.C. Sögütoglu, H.P. Huinink, H.R. Fischer, O.C.G. Adan, A review of salt hydrates for seasonal heat storage in domestic applications, Appl. Energy 199 (Aug. 2017) 45–68, https://doi.org/10.1016/j.apenergy.2017.04.080.

- [7] N. Mazur, et al., Revisiting salt hydrate selection for domestic heat storage applications, Renew. Energy 218 (Dec. 2023) 119331, https://doi.org/10.1016/j. renene.2023.119331.
- [8] A.D. Pathak, I. Tranca, S.V. Nedea, H.A. Zondag, C.C.M. Rindt, D.M.J. Smeulders, First-principles study of chemical mixtures of CaCl₂ and MgCl₂ hydrates for optimized seasonal heat storage, J. Phys. Chem. C 121 (38) (Sep. 2017) 20576–20590. https://doi.org/10.1021/acs.ipcc.7b05245.
- [9] W. Hua, H. Yan, X. Zhang, X. Xu, L. Zhang, Y. Shi, Review of salt hydrates-based thermochemical adsorption thermal storage technologies, J. Energy Storage 56 (Dec. 2022) 106158, https://doi.org/10.1016/j.est.2022.106158.
- [10] R.-J. Clark, M. Farid, Experimental investigation into the performance of novel SrCl2-based composite material for thermochemical energy storage, J. Energy Storage 36 (Apr. 2021) 102390, https://doi.org/10.1016/j.est.2021.102390.
- [11] H. Zondag, B. Kikkert, S. Smeding, R. de Boer, M. Bakker, Prototype thermochemical heat storage with open reactor system, Appl. Energy 109 (Sep. 2013) 360–365, https://doi.org/10.1016/j.apenergy.2013.01.082.
- [12] B. Michel, N. Mazet, P. Neveu, Experimental investigation of an open thermochemical process operating with a hydrate salt for thermal storage of solar energy: local reactive bed evolution, Appl. Energy 180 (Oct. 2016) 234–244, https://doi.org/10.1016/j.apenergy.2016.07.108.
- [13] A. Cosquillo Mejia, S. Afflerbach, M. Linder, M. Schmidt, Experimental analysis of encapsulated CaO/Ca(OH)2 granules as thermochemical storage in a novel moving bed reactor, Appl. Therm. Eng. 169 (Mar. 2020) 114961, https://doi.org/10.1016/ j.applthermaleng.2020.114961.
- [14] S. Salviati, F. Carosio, G. Saracco, A. Fina, Hydrated salt/graphite/polyelectrolyte organic-inorganic hybrids for efficient thermochemical storage, Nanomaterials 9 (3) (Mar. 2019) 420, https://doi.org/10.3390/nano9030420.
- [15] Q. Zhao, J. Lin, H. Huang, Z. Xie, Y. Xiao, Enhancement of heat and mass transfer of potassium carbonate-based thermochemical materials for thermal energy storage, J. Energy Storage 50 (Jun. 2022) 104259, https://doi.org/10.1016/j. est.2022.104259.
- [16] Y.J. Zhao, R.Z. Wang, Y.N. Zhang, N. Yu, Development of SrBr2 composite sorbents for a sorption thermal energy storage system to store low-temperature heat, Energy 115 (Nov. 2016) 129–139, https://doi.org/10.1016/j.energy.2016.09.013.
- [17] J. Aarts, B. Van Ravensteijn, H. Fischer, O. Adan, H. Huinink, Stabilization of salt hydrates using flexible polymeric networks, Energy 285 (Dec. 2023) 129540, https://doi.org/10.1016/j.energy.2023.129540.
- [18] W. Li, J.J. Klemeš, Q. Wang, M. Zeng, Development and characteristics analysis of salt-hydrate based composite sorbent for low-grade thermochemical energy storage, Renew. Energy 157 (Sep. 2020) 920–940, https://doi.org/10.1016/j. renepe.2020.05.062.
- [19] S.C. Akcaoglu, Z. Sun, S.C. Moratti, G. Martinopoulos, Investigation of novel composite materials for thermochemical heat storage systems, Energies 13 (5) (Feb. 2020) 1042, https://doi.org/10.3390/en13051042.
- [20] A.I. Shkatulov, J. Houben, H. Fischer, H.P. Huinink, Stabilization of K2CO3 in vermiculite for thermochemical energy storage, Renew. Energy 150 (May 2020) 990–1000. https://doi.org/10.1016/j.renene.2019.11.119.
- [21] J. Aarts, B. Van Ravensteijn, H. Fischer, O. Adan, H. Huinink, Polymeric stabilization of salt hydrates for thermochemical energy storage, Appl. Energy 341 (Jul. 2023) 121068, https://doi.org/10.1016/j.apenergy.2023.121068.
- [22] R. Fisher, Y. Ding, A. Sciacovelli, Hydration kinetics of K2CO3, MgCl2 and vermiculite-based composites in view of low-temperature thermochemical energy storage, J. Energy Storage 38 (Jun. 2021) 102561, https://doi.org/10.1016/j. est.2021.102561.
- [23] F. Ye, D. Bo, Study on long-term thermochemical thermal storage performance based on SrBr2-expanded vermiculite composite materials, J. Energy Storage 42 (2021) 103081.
- [24] Y.N. Zhang, R.Z. Wang, Y.J. Zhao, T.X. Li, S.B. Riffat, N.M. Wajid, Development and thermochemical characterizations of vermiculite/SrBr2 composite sorbents for low-temperature heat storage, Energy 115 (Nov. 2016) 120–128, https://doi.org/ 10.1016/j.energy.2016.08.108.
- [25] V. Brancato, et al., MgSO4-7H2O filled macro cellular foams: an innovative composite sorbent for thermo-chemical energy storage applications for solar buildings, Sol. Energy 173 (Oct. 2018) 1278–1286, https://doi.org/10.1016/j. solener.2018.08.075.
- [26] L.-C. Sögütoglu, et al., Understanding the hydration process of salts: the impact of a nucleation barrier, Cryst. Growth Des. 19 (4) (Apr. 2019) 2279–2288, https://doi. org/10.1021/acs.cgd.8b01908.
- [27] J. Houben, D. Langelaan, L. Brinkman, H. Huinink, H.R. Fischer, O.C.G. Adan, Understanding the hydration process of salts: the relation between surface mobility and metastability, Cryst. Growth Des. 22 (8) (Aug. 2022) 4906–4916, https://doi. org/10.1021/acs.cgd.2c00416.
- [28] M. Beving, J. Romme, P. Donkers, A. Frijns, C. Rindt, D. Smeulders, Experimental and numerical validation of the one-process modeling approach for the hydration of K2CO3 particles, Processes 10 (3) (Mar. 2022) 547, https://doi.org/10.3390/ px10030547
- [29] M.A.J.M. Beving, A.J.H. Frijns, C.C.M. Rindt, D.M.J. Smeulders, Effect of cycle-induced crack formation on the hydration behaviour of K2CO3 particles: experiments and modelling, Thermochim. Acta 692 (Oct. 2020) 178752, https://doi.org/10.1016/j.tca.2020.178752.
- [30] K. Linnow, M. Niermann, D. Bonatz, K. Posern, M. Steiger, Experimental studies of the mechanism and kinetics of hydration reactions, Energy Procedia 48 (2014) 394–404, https://doi.org/10.1016/j.egypro.2014.02.046.
- [31] M. Gaeini, S.A. Shaik, C.C.M. Rindt, Characterization of potassium carbonate salt hydrate for thermochemical energy storage in buildings, Energy Build. 196 (Aug. 2019) 178–193, https://doi.org/10.1016/j.enbuild.2019.05.029.

- [32] M.A. Stanish, D.D. Perlmutter, Kinetics of hydration-dehydration reactions considered as solid transformations, AICHE J. 30 (4) (Jul. 1984) 557–563, https://doi.org/10.1002/aic.690300405.
- [33] A. Martin, D. Lilley, R. Prasher, S. Kaur, Particle size optimization of thermochemical salt hydrates for high energy density thermal storage, Energy Environ. Mater. (Feb. 2023) e12544, https://doi.org/10.1002/eem2.12544.
- [34] N. Mazur, H. Huinink, H. Fischer, P. Donkers, O. Adan, Accelerating the reaction kinetics of K2CO3 through the addition of CsF in the view of thermochemical heat storage, Sol. Energy 242 (Aug. 2022) 256–266, https://doi.org/10.1016/j. solener.2022.07.023.
- [35] J. Houben, J. van Biesen, H. Huinink, H. R. Fischer, and O. C. G. Adan, "Accelerating the hydration reaction of potassium carbonate using organic dopants".
- [36] A. Khawam, D.R. Flanagan, Solid-state kinetic models: basics and mathematical fundamentals, J. Phys. Chem. B 110 (35) (Sep. 2006) 17315–17328, https://doi. org/10.1021/jp062746a.
- [37] S. Vyazovkin, A.K. Burnham, J.M. Criado, L.A. Pérez-Maqueda, C. Popescu, N. Sbirrazzuoli, ICTAC kinetics committee recommendations for performing kinetic computations on thermal analysis data, Thermochim. Acta 520 (1–2) (Jun. 2011) 1–19, https://doi.org/10.1016/j.tca.2011.03.034.
- [38] B. Kieskamp, A. Mahmoudi, M. Shahi, A novel multi-reactor system for thermochemical heat storage through detailed modeling of K2CO3 particles, J. Energy Storage 78 (Feb. 2024) 110028, https://doi.org/10.1016/j. est.2023.110028.
- [39] L.-C. Sögütoglu, F. Birkelbach, A. Werner, H. Fischer, H. Huinink, O. Adan, Hydration of salts as a two-step process: water adsorption and hydrate formation, Thermochim. Acta 695 (Jan. 2021) 178819, https://doi.org/10.1016/j. tca.2020.178819.
- [40] J. Aarts, et al., Diffusion limited hydration kinetics of millimeter sized salt hydrate particles for thermochemical heat storage, J. Energy Storage 47 (Mar. 2022) 103554, https://doi.org/10.1016/j.est.2021.103554.
- [41] P. Atkins, J. De Paula, Atkins' Physical Chemistry, 9th ed., Oxford University Press,

- [42] L.-C. Sögütoglu, Fundamentals of salt hydration for heat battery application. Technische Universiteit Eindhoven.
- [43] N. Mazur, et al., Impact of polymeric stabilisers on the reaction kinetics of SrBr2, Sol. Energy Mater. Sol. Cells 238 (May 2022) 111648, https://doi.org/10.1016/j. solmat 2022 111648.
- [44] L. Greenspan, Humidity fixed points of binary saturated aqueous solutions, J. Res. Natl. Bur. Stand. Sect. Phys. Chem. 81A (1) (Jan. 1977) 89, https://doi.org/ 10.6028/jres.081A.011.
- [45] M. Dyke, R.L. Sass, The crystal structure of strontium bromide monohydrate, J. Phys. Chem. 68 (11) (Nov. 1964) 3259–3262, https://doi.org/10.1021/ i100793a031.
- [46] E. Vordemvenne, I. Abrahams, Strontium Dibromide Hexahydrate vol. C51, 1995, pp. 183–185, https://doi.org/10.1107/S0108270194010796.
- [47] T. Echigo, M. Kimata, A. Kyono, M. Shimizu, T. Hatta, Re-investigation of the Crystal Structure of Whewellite [Ca(C2O4)·H2O] and the Dehydration Mechanism of Caoxite [Ca(C2O4)·3H2O] vol. 69, no. 1, 2005, pp. 77–88, https://doi.org/ 10.1180/0026461056910235.
- [48] O. Hochrein, A. Thomas, R. Kniep, Revealing the crystal structure of anhydrous calcium oxalate, $Ca[C_2O_4]$, by a combination of atomistic simulation and Rietveld refinement, Z. Anorg. Allg. Chem. 634 (11) (Sep. 2008) 1826–1829, https://doi.org/10.1002/zaac.200800207.
- [49] M. Steiger, et al., Hydration of MgSO4-H2O and generation of stress in porous materials, Cryst. Growth Des. 8 (1) (Jan. 2008) 336–343, https://doi.org/10.1021/ cg060688c.
- [50] Handbook of Chemistry and Physics, 95th ed., CRC Press, 2015.
- [51] C. Pichler, R. Lackner, T. Bader, L. Perfler, Water vapor diffusion properties of Obernkirchener sandstone: analysis of DVS data, Constr. Build. Mater. 347 (Sep. 2022) 128554, https://doi.org/10.1016/j.conbuildmat.2022.128554.
- [52] J.D. Jabro, Water vapor diffusion through soil as affected by temperature and aggregate size, Transp. Porous Media 77 (3) (Apr. 2009) 417–428, https://doi.org/ 10.1007/s11242-008-9267-z.
- [53] L. Glasser, Thermodynamics of inorganic hydration and of humidity control, with an extensive database of salt hydrate pairs, J. Chem. Eng. Data 59 (2) (Feb. 2014) 526–530, https://doi.org/10.1021/je401077x.